Available online at www.sciencedirect.com

ScienceDirect

Energy Procedia 137 (2017) 539–552

Energy Procedia

www.elsevier.com/locate/procedia

14th Deep Sea Offshore Wind R&D Conference, EERA DeepWind'2017, 18-20 January 2017, Trondheim, Norway

An engineering model for dynamic wind power plant flow

Karl O. Merz[a,*]

[a]*SINTEF Energy Research, Sem Sælands vei 11, Trondheim, 7034, Norway*

Abstract

An engineering method is developed for the prediction of dynamic flow through a wind power plant, in the presence of turbine control actions. The model is composed of a simplified steady-state boundary layer model of velocity deficits and turbulence, a dynamic wake model relating the rotor induction to an effective "dynamic" value of thrust, and a flow convection model which is simply a time delay function. A partial validation is conducted, using wake measurements at the Nørrekær Enge wind farm. The model is implemented in the STAS WPP program for wind power plant analysis.

Peer-review under responsibility of SINTEF Energi AS.

Keywords: wind farm; wind power plant; control; wakes

1. Introduction

To study the control of a wind power plant requires a model for the atmospheric flow, which is coupled with the operation of the wind turbines. There are two rather distinct flow regimes [1]. On the upwind side of the turbine array, a concentrated wake forms behind individual wind turbines, and this may impinge, or not, on the turbines immediately downwind. These local wakes are often modelled by a Gaussian-shaped velocity deficit [2], which decays as higher-velocity air is entrained by turbulent mixing. Deep in a large wind power plant, there are still local wakes, but the presence of the wind turbines is also felt throughout the atmospheric boundary layer, to an elevation much higher than the tops of the rotors. Energy recovery occurs "top-down" as higher-velocity air in the upper portion of the boundary layer is mixed into the lower levels.

* Corresponding author. Tel.: +47 91801670.
E-mail address: karl.merz@sintef.no

1876-6102
Peer-review under responsibility of SINTEF Energi AS.
10.1016/j.egypro.2017.10.383

Interestingly, methods based on boundary-layer analysis provide good predictions of the average velocity deficits, even near the upwind side of a wind power plant [1,3]. That is, the local wakes may meander back and forth, with the second row of turbines seeing a velocity deficit which fluctuates abruptly [4]; yet in the mean, the boundary layer experiences the turbines as, effectively, an increased surface roughness, like a forest canopy [5]. The influence of the local wake on stochastic loads may be approximated by an increased turbulence intensity [6].

The goal is to assemble, from existing parts, a simple engineering method for predicting the influence of turbine control actions on the flow through a wind power plant. The method must be compatible with a state-space model of the turbines, electrical grid, and controls comprising the wind power plant. CFD analyses of the complete flow domain are ruled out, for the time being. This leaves an approach based on one or both of the above perspectives: superposition of local wakes, or a simplified boundary-layer analysis.

Here it is proposed to use a method based partly on a two-dimensional boundary-layer analysis, specifically the Viper software [3]. The boundary-layer approach has the advantages of being scalable from small turbine arrays to large wind power plants, or even plant clusters; and of not attempting to explicitly resolve the local wake, where the result becomes sensitive to small changes in the wind direction. In other words, the control algorithms so developed will be applicable in bulk, rather than for specific wind directions.

2. State-space representation of flow

A state-space model of the flow is built up from the following elements:

a. The dynamic induced velocity, which is obtained from Øye's second-order filter model [7], built into the STAS Turbine module [8]. The second-order filter, like the real wake dynamics, has the feature that rapid control inputs have little influence on the wake flow: the amplitude decays with frequency in a realistic manner. †
b. A steady-state boundary layer analysis [3] relating the induction at an upwind location to the velocity deficit at a downwind location.
c. A convection model for signals (velocity deficits) in the flow. Convection is modelled as a state-space approximation of a time delay, based on the hub-height windspeed. As simple as the time-delay assumption is, it has been validated by wind tunnel experiments [10].
d. A model for the effective turbulence intensity including wake effects, based on Frandsen [6].

2.1. Transient induction and the boundary layer

Let us begin the story with the induced velocity, and its connection to the flow, in the context of boundary layer analysis. Momentum balance applied to a control volume of air flowing through the rotor gives the well-known relationship

$$C_T = 4a(1-a), \qquad C_T := \frac{F_T}{(1/2)\rho A V_\infty^2}, \quad a := -\frac{V_i}{V_\infty} \tag{1}$$

or equivalently

$$F_T = -2\rho A(V_\infty + V_i)V_i \tag{2}$$

The theoretical relation (1) must be augmented with an empirical trend for values of a above about 0.4. Burton et al. [11] propose a linear trend,

---

† A manuscript by Pedersen [9] provides an excellent description of the pattern of vorticity in the wake, and distribution of the induced velocity over the rotorplane, under control inputs of various frequencies.

$$C_T = \frac{a - a_1}{a_2 - a_1}\left(C_{T2} - C_{T1}\right) + C_{T1}, \qquad (3)$$

$$a_2 = 1, \qquad C_{T2} = 1.82, \qquad a_1 = 1 - \frac{\sqrt{C_{T2}}}{2}, \qquad C_{T1} = 4a_1\left(1 - a_1\right)$$

Alternative formulas for (3) are also available. Regardless, the main point here is that for steady flow there is a 1:1 correspondence between the rotor-average induced velocity and the thrust.

The relationships (1) through (3) between induced velocity and thrust do not hold under transient conditions. The induced velocity lags changes in the rotor loading, with an amplitude that decreases at high frequencies. Physically, this is due to the time it takes to convect the wake vorticity – which is responsible for the induced velocity – downstream away from the rotor. A slow fluctuation in the rotor load gives the wake time to develop, and the induced velocity follows the steady-state trend. A fast fluctuation in the rotor load produces a pattern of vorticity in the wake whose net effect tends to cancel out, except near the tips of the blades. A method attributed to S. Øye, described by Snel & Schepers [7], captures these trends by a second-order filter,

$$\frac{ds}{dt} = -\frac{1}{\tau_1}s + \frac{0.4}{\tau_1}V_i, \qquad \frac{d\bar{V}_i}{dt} = -\frac{1}{\tau_2}\bar{V}_i + \frac{1}{\tau_2}s + \frac{0.6}{\tau_2}V_i \qquad (4)$$

$$\tau_1 = \frac{1.1}{1 - 1.3a}\left(\frac{D}{2V_\infty}\right), \qquad \tau_2 = \left[0.39 - 0.26\left(\frac{2r}{D}\right)^2\right]\tau_1$$

Here V_i satisfies (2) instantaneously, whereas the filtered $\bar{V}_i$ is taken as the true value at the rotorplane. The time constants in (4) are a function of the radius, but the equations may be integrated, or an effective value at $r/R \approx 0.7$ taken, in order to represent the rotor average.

This same line of thought can be extended to boundary-layer analysis. Namely, that a slow fluctuation in the rotor load will produce a well-developed wake which, upon subsequent breakup and diffusion of the momentum deficit, will influence the atmospheric boundary layer; whereas a fast fluctuation in the rotor load will lead to local features in the flow which will tend to cancel out, from the broader perspective of the boundary layer. To put it another way, we connect the development of the boundary layer with the wake, represented by the induction, and not the instantaneous loading on the rotor. We suggest the use of (4) to obtain $\bar{V}_i$, and then (2) to obtain a "wake-equivalent" value of rotor thrust,

$$\bar{F}_T = -2\rho A\left(V_\infty + \bar{V}_i\right)\bar{V}_i \qquad (5)$$

which is experienced by the boundary layer.

2.2. Steady-state perturbations in the boundary layer

To the extent that the boundary layer is influenced by the rotor thrust $\bar{F}_T$, or equivalently $\bar{V}_i$, this decays with the distance downstream. In other words, if one should begin with a boundary layer in a steady-state condition, make a constant perturbation to the rotor thrust $F_T = \bar{F}_T$ at some location, and allow the flow to reach a new steady state, then the velocity profile of the perturbed flow will asymptotically approach the original, far downstream. The decay is due to the fact that, given a uniform rotor thrust loading, the boundary layer tends to reach an equilibrium over long distances. At equilibrium, the turbulent diffusion of momentum from the high-velocity air at altitude balances the momentum removed by the rotor thrust and surface friction. The higher the loading on the air at low altitudes, the greater the shear in velocity with height, and the greater the mixing in of momentum from above.

As an illustration, consider a wind power plant consisting of a uniform grid of DTU 10 MW wind turbines [12], with spacing $s_x = s_z = 8D$. (The X direction is along-wind, the Z direction is cross-wind, and the Y direction is straight up.) The remote incoming windspeed is 10 m/s. Figure 1 shows the hub-height velocity profile from the first through the 21st row of turbines. The velocity profile as a function of height, just upstream of Turbine Row 6, is also shown. The effect of shutting down Turbine Row 5 is illustrated by the dashed curves. Immediately downstream there is recovery of windspeed, which diminishes far downstream as the boundary layer approaches equilibrium.

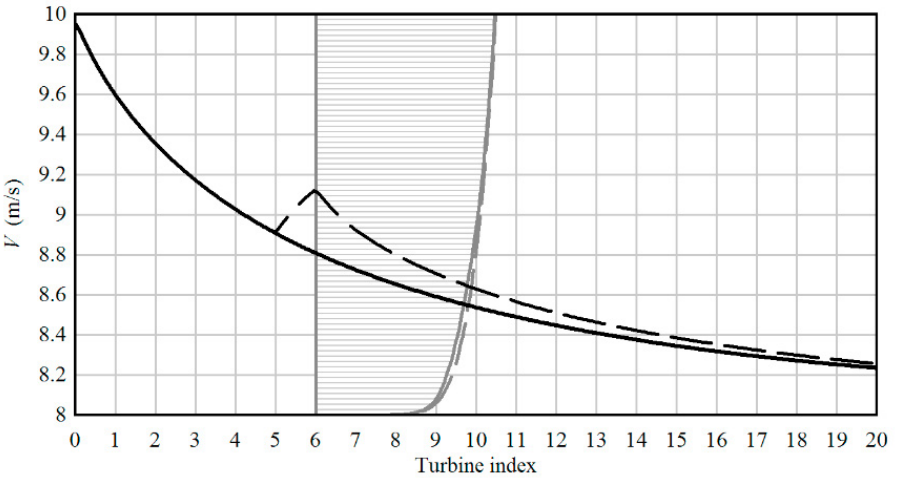

Figure 1: The hub-height velocity, and the velocity profile with altitude at Turbine Row 6, for two scenarios: one in which all the turbines are operating normally, and another (dashed lines) in which Turbine Row 5 is shut down. The velocity profile with altitude (shaded gray) does not correspond to the units on the axes. For an idea of scale, the uppermost elevation shown is 500 m, and the windspeed at 500 m is about 10.9 m/s.

The profiles in Fig. 1 are generated by solving nonlinear differential equations for a turbulent boundary layer. In order to make a useful low-order state-space model of the boundary-layer flow, we must identify simple linear models that capture the effect of perturbations about a given operating condition. Intuitively, and consistent with elementary boundary-layer theory, we can say that the perturbation in hub-height windspeed seen by the k^{th} turbine is some function of the loading, or induction, of the upstream turbines. Assuming that this relationship is linear for small enough perturbations,

$$\delta V_k = \frac{\partial V_k}{\partial V_{i,1}} \delta V_{i,1} + \frac{\partial V_k}{\partial V_{i,2}} \delta V_{i,2} + \ldots + \frac{\partial V_k}{\partial V_{i,k-1}} \delta V_{i,k-1} \tag{6}$$

Equation (6) is global, in the sense that in order to solve for δV_k we would need to know all the influence coefficients $\partial V_k / \partial V_{i,j}$ and induced velocities $\delta V_{i,j}$ for the upstream turbines. In the steady-state case, this is a computation involving a lower-triangular matrix, which is no problem. However, it becomes a problem in the dynamic case, because there is a unique time delay between each upstream-downstream pair of turbines; and, as will be seen in Section 2.3, an accurate representation of a long time delay requires a lot of states.

It is much more convenient if we can write

$$\delta V_k = \frac{\partial V_k}{\partial V_{k-1}} \delta V_{k-1} + \frac{\partial V_k}{\partial V_{i,k-1}} \delta V_{i,k-1} \tag{7}$$

That is, if we associate with each wind turbine an incoming windspeed V_k and a (downstream-side) induced velocity $V_{i,k}$, and say that the windspeed at the next turbine downstream is a function of these. Indeed, (6) is recovered from (7), provided that

$$\frac{\partial V_k}{\partial V_{i,j}} = \frac{\partial V_k}{\partial V_{k-1}} \frac{\partial V_{k-1}}{\partial V_{k-2}} \cdots \frac{\partial V_{j+2}}{\partial V_{j+1}} \frac{\partial V_{j+1}}{\partial V_{i,j}} \tag{8}$$

and $\delta V_1 = 0$. In other words, (8) holds true if the decay in a perturbation is multiplicative as one proceeds from station to station downstream.

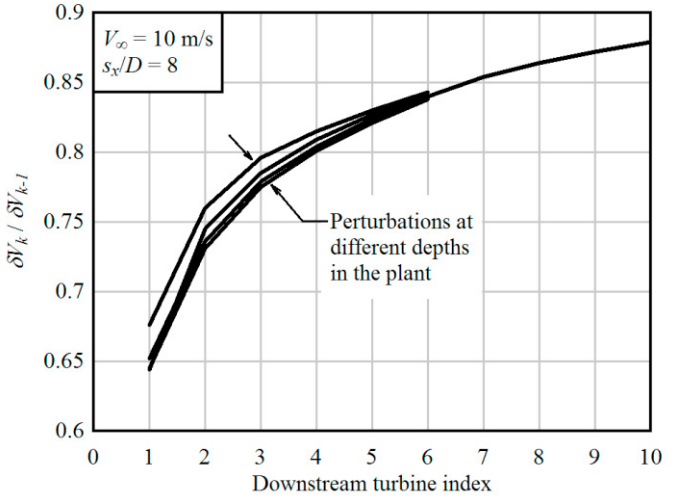

Figure 2: The station-to-station decay of a perturbation to the boundary layer. Multiple analyses were run, each time perturbing the operation of a different wind turbine. The downstream turbine index indicates the location relative to the turbine whose operation was perturbed. The trend is relatively independent of the depth in the wind power plant.

As it turns out, this is not strictly true; but it is close enough to be a useful assumption. Furthermore, the influence of a perturbation in turbine operating state $\delta V_{i,k}$ appears to be nearly independent of the downstream location. To illustrate this, consider again the example of a 10 m/s remote windspeed and a uniform 8D spacing. Figure 2 shows the results of introducing a perturbation in the operation of a wind turbine – specifically, decreasing the thrust by 10%. Referring to the indices of Fig. 2, the operation of Turbine -1 is perturbed, such that Turbine 0 experiences a change in the incoming windspeed

$$\delta V_0 = \frac{\partial V_0}{\partial V_{i,-1}} \delta V_{i,-1} \tag{9}$$

The curve shows subsequent values of $\partial V_k/\partial V_{k\text{-}1}$ for k = 1,2,… The trend is nearly independent of the location in the plant at which the perturbation is introduced. The trend is also independent of the amplitude: Fig. 3 shows reductions in thrust from 10% to 100% (shut down turbine).

The value of $\partial V_k/\partial V_{i,k\text{-}1}$ is also remarkably consistent, and is equal to about 0.08 in the case of a 10 m/s remote windspeed and a uniform 8D spacing.

Still, Fig. 2 and Fig. 3 are not enough. If $\partial V_k/\partial V_{k\text{-}1}$ is a function of the downstream turbine index – relative to where the perturbation was introduced – then one still must formulate individual values for each upstream-downstream combination of turbines. We really need $\partial V_k/\partial V_{k\text{-}1}$ to be constant, such that we can say how the perturbation to the windspeed $\delta V_{k\text{-}1}$ will evolve downstream into δV_k, independent of how $\delta V_{k\text{-}1}$ was created. If we take the approximation $\partial V_k/\partial V_{k\text{-}1} \approx 0.75$, then this provides a good estimate of the flow over a distance of several turbines downstream of the perturbation. In addition, superposition applies. Figure 4 shows an example where the thrust of turbines 2, 5, and 10 has been reduced. The perturbation in hub-height windspeed is well-predicted by (7), with a constant $\partial V_k/\partial V_{k\text{-}1}$; except that the perturbation decays too fast far downstream.

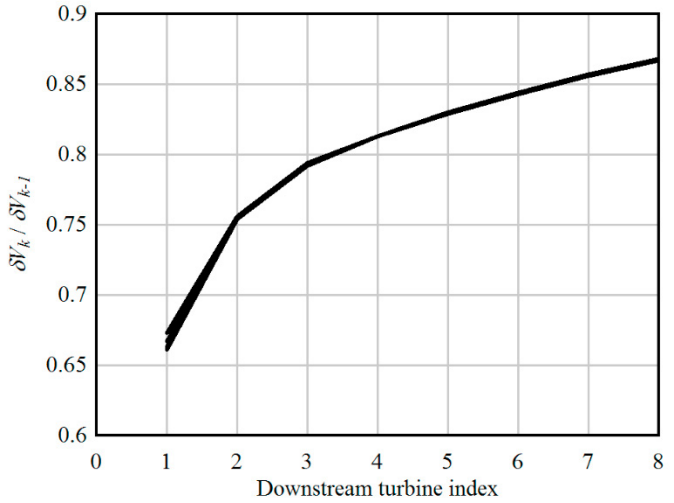

Figure 3: The influence, or lack thereof, of the perturbation amplitude on the trend in the station-to-station decay of the perturbed velocity.

The values of $\partial V_k/\partial V_{k\text{-}1}$ and $\partial V_k/\partial V_{i,k\text{-}1}$ may depend on the size of the wind turbine, the remote windspeed, and the spacing between turbines, and should be generated, or obtained from a database, for each load case being analyzed.

2.3. Convection of flow perturbations

The transmission of a signal – that is, a perturbation in the flow – from an upwind to a downwind turbine can be modelled as convection at the hub-height windspeed [10]. The frequency dependence is handled by the dynamic wake method of Section 2.1, while the diffusion part is handled by the boundary-layer calculations – or the simplified approximation – of Section 2.2. The convection model is therefore a pure time delay.

A time delay of τ is simple to model as a transfer function,

$$\frac{dy}{dx} = \exp(-s\tau) \tag{10}$$

simple to model in (discrete) time domain simulations,

$$y(t) = x(t-\tau) \tag{11}$$

although $x(T)$ must be stored for $t - \tau \le T \le t$; and difficult to model in state space. The storage requirement for (11) hints at the problem. How many values are required to store a segment of a continuous function? An infinite number; that is, an infinite number of states is required in order to represent (10) or (11) exactly. With a finite number of states, a time delay may be approximated by a rational transfer function,

$$\frac{dy}{dx} \approx \frac{P_m(s\tau)}{Q_n(s\tau)} \tag{12}$$

$$P_m(x) = \sum_{k=0}^{m} \frac{(m+n-k)!m!}{(m+n)!(m-k)!k!}(-x)^k, \quad Q_n(x) = \sum_{k=0}^{n} \frac{(m+n-k)!n!}{(m+n)!(n-k)!k!}x^k$$

It is common to use $m = n$, as this gives a transfer function with a uniform unit amplitude. The alternative, $m < n$, results in a low-pass behavior.

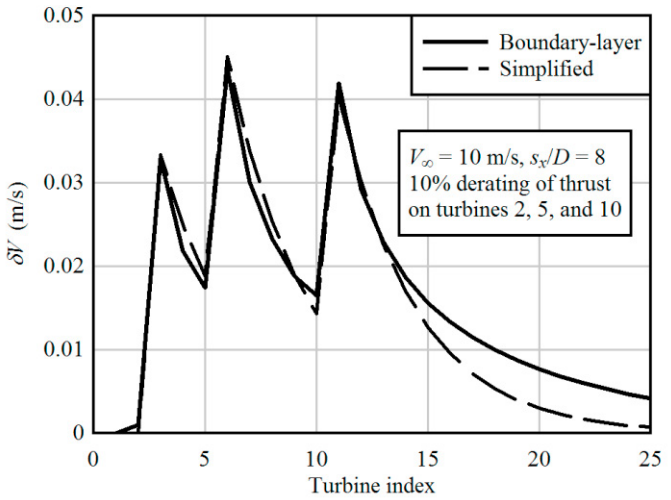

Figure 4: The approximation to the perturbed velocity that is obtained from (7), compared with the full boundary-layer analysis, for a case with multiple perturbations.

The higher the frequency of the signal to be transmitted, in relation to the delay time, the more states are required. The use of too few states, for a given frequency and time delay, will either transmit the signal with insufficient lag ($m = n$), or transmit nothing ($m < n$). Our situation is unfortunately one in which the time delay is long in comparison with the timescale of the signal. The latter is the timescale of the dynamic wake, which can be obtained from (4). (Higher frequencies are negligible due to the low-pass behavior.) In the present example of a 10 MW wind turbine, $\tau_1 \approx 16$ s. If the spacing between turbines is $8D$, or 1426 m, and the windspeed is 10 m/s, then the time delay is 143 s, an order-of-magnitude greater. We now see why it is so important to use (7), instead of (6), even at the expense of some accuracy: we do not want to track a velocity perturbation over a distance farther than the separation between turbines.

A state-space form of (12), for $m = n$, is

$$\frac{d}{dt}\begin{bmatrix} x_1 \\ x_2 \\ \vdots \\ x_n \end{bmatrix} = \begin{bmatrix} 0 & 1 & & 0 \\ 0 & 0 & & 0 \\ & & \ddots & \\ -q_0/q_n & -q_1/q_n & & -q_{n-1}/q_n \end{bmatrix}\begin{bmatrix} x_1 \\ x_2 \\ \vdots \\ x_n \end{bmatrix} + \begin{bmatrix} 0 \\ 0 \\ \vdots \\ 1 \end{bmatrix} u \qquad (13)$$

$$y = \frac{p_n}{q_n}\begin{bmatrix} p_0/p_n - q_0/q_n & p_1/p_n - q_1/q_n & \cdots & p_{n-1}/p_n - q_{n-1}/q_n \end{bmatrix}\begin{bmatrix} x_1 \\ x_2 \\ \vdots \\ x_n \end{bmatrix} + \frac{p_n}{q_n} u$$

At high orders n – say, 10 or higher – (13) exhibits poor numerical conditioning. This effectively limits the bandwidth. Continuing with the example of a 10 m/s windspeed and $8D$ spacing, Fig. 5 compares the phase angle obtained using different orders of (13) against the exact value $\theta = -\omega s_x/V_\infty$. The maximum condition number C of the matrix $i\omega\mathbf{I} - \mathbf{A}$, representing a frequency-domain solution of the state equations, is also listed. This condition number is that obtained after employing a balancing operation, intended to improve the numerical conditioning.

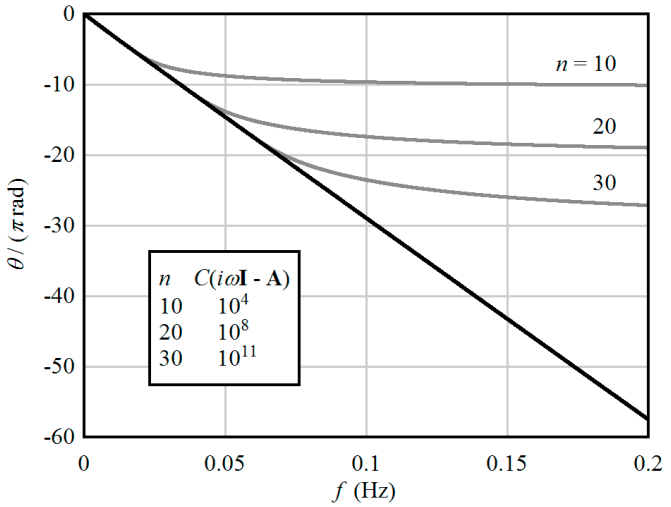

Figure 5: The phase angle, in multiples of π, of the time delay $\exp(-i\omega s_x/V_\infty)$, compared against different orders of the approximation (13)

The numerical conditioning can be greatly improved by breaking the spacing s_x between wind turbines into sub-intervals, and employing a low-order form of (13) over each sub-interval. The downside is an increase in the number of states required for a given accuracy of approximation.

The time delay must be accurately represented over the bandwidth of the wake dynamics. Figure 6 plots the magnitude of the transfer function $\partial\bar{V}_i/\partial V_i$ from (4). A reasonable criterion for accuracy is, say, that the phase of the time delay is within 1% of the exact value at a frequency of 0.1 Hz. Phase errors at a higher frequency than this will have a limited influence on the dynamic response of the wind turbines, since the relative magnitude of the velocity perturbations is small.

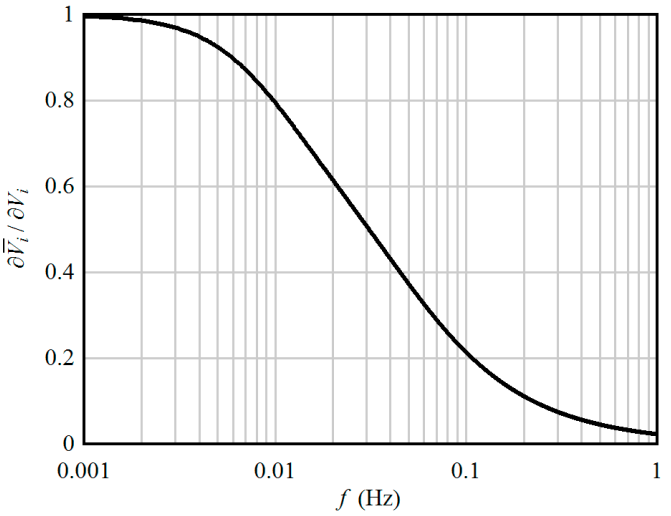

Figure 6: The magnitude of the transfer function between steady-state and transient induced velocity, according to (4), for a windspeed of 10 m/s.

Table I shows combinations of the number of sub-intervals N_s and the order of approximation n from (13) that satisfy the stated criterion for accuracy. The condition number is also shown. Increasing the number of sub-intervals improves the numerical conditioning. An increased number of states is required; but this has the additional benefit, seen in Fig. 7, that the accuracy is improved at higher frequencies.

Table I: Combinations of the number of sub-intervals N_s and order of approximation n that satisfy the criterion for accuracy.

N_s	n	N_x	$C(i\omega\mathbf{I}-\mathbf{A})$
2	27	54	10^7
3	19	57	10^6
4	15	60	10^5
5	13	65	10^4
6	11	66	10^4
7	10	70	10^4
8	9	72	10^4
10	8	80	10^4
12	7	84	10^4
15	6	90	10^3
19	5	95	10^3
28	4	112	10^3
49	3	147	10^3

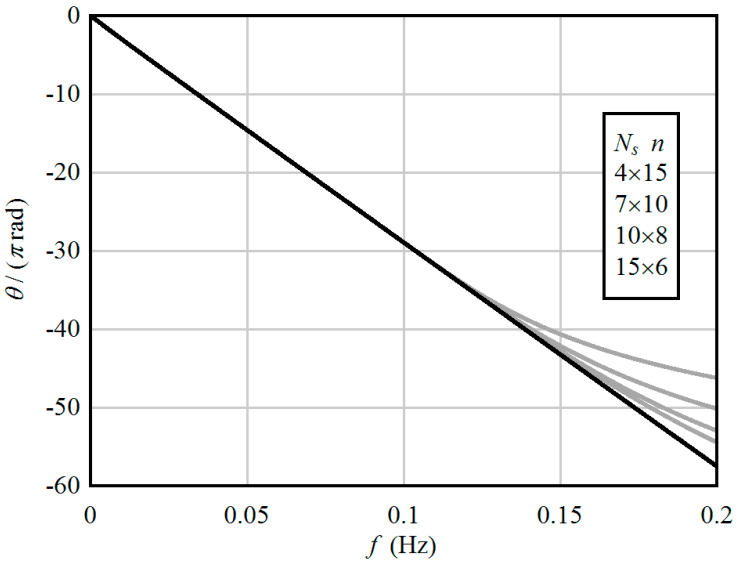

Figure 7: The approximate and true phase of a time delay, with various numbers of sub-intervals and orders of approximation, satisfying the criterion that the error in phase is less than 1% at a frequency of 0.1 Hz.

2.4. Turbulence

The level of turbulence within a wind power plant is a function of the terrain, atmospheric conditions, and turbine operation. Terrain effects are specific to each location; here we assume that the terrain is flat enough that its influence can be represented by an empirical surface roughness length y_0. Then, under conditions of neutral stability (no thermal convection or stabilization), the standard deviation of turbulent velocity fluctuations can be estimated as [6]

$$\sigma_v \approx h\frac{\partial V}{\partial h} \tag{14}$$

where h is the elevation above the ocean or land surface. In other words, if we know the wind shear $\partial V/\partial h$, then we may directly estimate the level of turbulence. The velocity profile with height, and hence the wind shear, is computed as part of the steady-state boundary-layer analyses of Section 2.2.

Figure 8 shows an example of the levels of turbulence so obtained. The ambient value of the turbulence intensity is about 8%. Deep inside the wind power plant, it is around 13% to 14%, depending on how the effective value is computed from the profile. These values of turbulence intensity are based on the local mean hub-height windspeed, which is lower than the ambient value upwind of the turbine array. Relative to the ambient hub-height windspeed, the turbulence intensity is about 12%, which is in agreement with the value given by Frandsen [6] for an infinitely large turbine array.

If the level of turbulence follows from the velocity profile, and the profile is convected dynamically at the mean hub-height windspeed, then it can be assumed that under dynamic conditions, the level of turbulence evolves according to the time delay functions of Section 2.3.

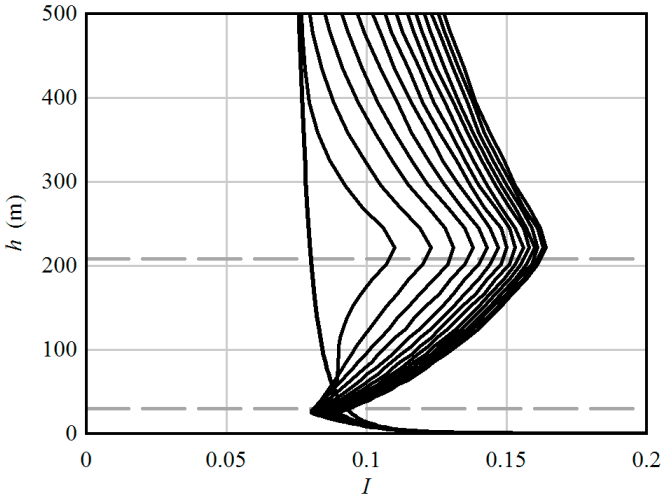

Figure 8: The turbulence intensity as a function of height, for turbines progressively deeper inside a large wind power plant. Here $V_\infty = 10$ m/s, $s_x/D = 8$, and $y_0 = 0.001$ m. The dashed gray lines indicate the bottom and top elevations of the rotor.

2.5. Preliminary comparison with data

The Nørrekær Enge wind power plant, described by Hansen [13], offers a partial field validation of the simple turbulence model (14). Frandsen [6] provides some normalized windspeed and turbulence measurements, as a function of elevation, for wind directions within ±15° of southwest. The plant layout is sketched in Fig. 9, with the axes in units of meters from the met mast at which data was collected. Two-dimensional boundary-layer analysis was performed along three lines: one oriented to the southwest, and one each at ±15°. Profiles of windspeed and turbulence intensity were obtained as averages from these three lines, weighting the middle line twice.

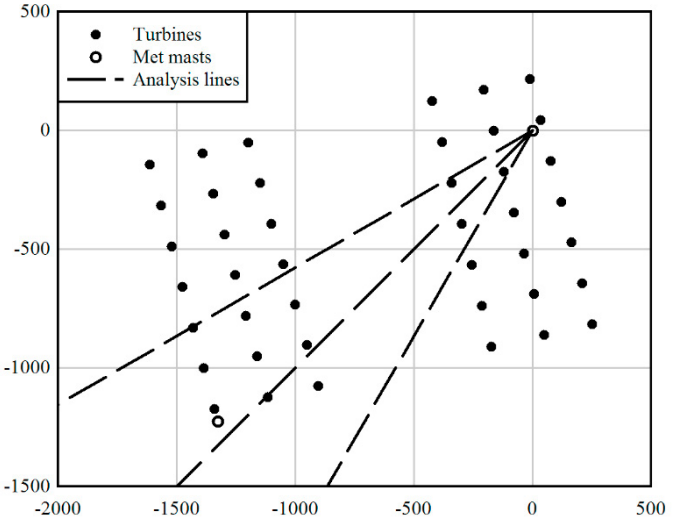

Figure 9: The layout of the Nørrekær Enge wind power plant, showing the met masts and lines along which boundary-layer analyses were conducted.

The measured and computed profiles are plotted in Fig. 10. There is some uncertainty in both the data and the analysis. In the case of the data, Frandsen gives profiles with height for ambient windspeed ranges of 8-9 m/s (plot at left) and 12-14 m/s (plot at right), and subsequently the same values at a single elevation of 58 m, for integer windspeeds between cut-in and cut-out. The values do not exactly agree, and no explanation is offered; presumably, they were based on different sets of measurements. Uncertainty in the analysis is related to the effective surface roughness length. The wind farm was located in grassy terrain. Some kilometers upstream the terrain was hilly, and closer upstream there were obstacles such as farm buildings. For comparison, the analysis was run with roughness values of 0.03 m, representative of flat grassy terrain, and 0.2 m, representative of hedges.

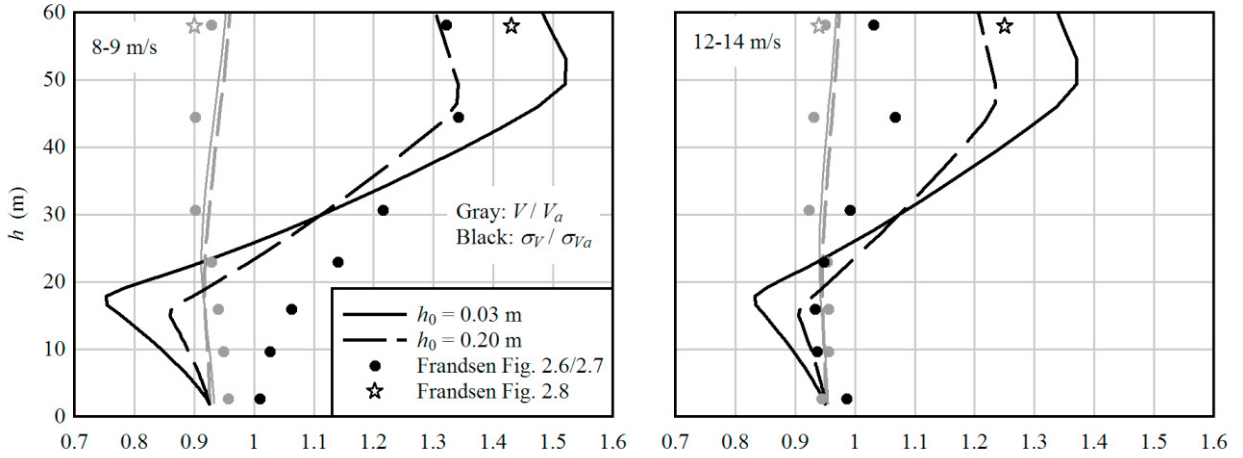

Figure 10: Windspeed and turbulence profiles as a function of elevation, presented as a ratio of the value measured within the wind turbine array to that measured immediately upstream of the array.

Overall, the comparisons in Fig. 10 indicate that the simplified boundary-layer analysis predicts reasonable trends in the development of wake velocity deficits and turbulence in a wind power plant. At the same time, there are clearly factors which influence the atmospheric flow, which are not taken into account.

Wind tunnel tests [14] also exhibit the pattern of turbulence predicted in Fig. 10. A full validation exercise is left to future work.

3. Steady-state power set-points

Consider the problem of optimizing the pitch – or equivalently, the axial induction – of an array of wind turbines, in order to maximize the total production. Simplified methods based on local wake analysis, such as Jensen [15] and its derivatives, predict that the maximum power is obtained when the production of the upstream turbines is curtailed [16]. On the other hand, recent analyses using large eddy simulation [17] fail to reproduce this result: the maximum power of a two-turbine pair is obtained when both turbines are set to their respective maximum aerodynamic efficiencies. It is of interest to see how boundary-layer methods fare.

According to the methods of Section 2, each turbine is represented as a distributed thrust over an equivalent volume of air. Lateral mixing of the wake is assumed to be negligible in comparison with vertical mixing, giving a two-dimensional boundary-layer flow. In the case considered, the layout consists of DTU 10 MW wind turbines arranged with a uniform 8D spacing, and the ambient windspeed is 10 m/s.

Figure 11 shows the results for a single upwind/downwind turbine pair. In this case, curtailing the operation of the upwind turbine is always detrimental to the total production.

On the other hand, for a large wind power plant consisting of many rows of turbines, curtailing the operation of the upwind turbines may provide a slight benefit. Table II compares the baseline and optimal blade pitch set-points, to the nearest 0.2°, for a wind power plant with 11 turbine rows. The total power output is increased 0.5% by derating the upwind turbines. The turbulence intensity is also decreased by a couple percent. This hints that there may be something to be gained from the strategy; though the margin of uncertainty in the analysis is larger than the potential effect.

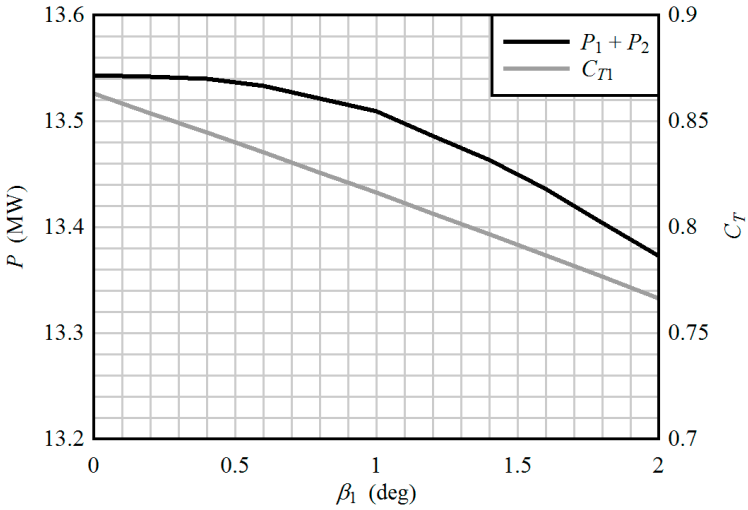

Figure 11: Axial induction control of a single upwind/downwind pair of turbine rows, according to the distributed-thrust boundary layer model of flow through a wind power plant.

4. Conclusions

An engineering method has been developed for predicting the influence of control actions on the flow through a wind power plant. The physics are simplified, not by superposing axisymmetric wakes as in Jensen-type methods [15], but by representing the turbines as a distributed drag on the atmospheric boundary layer. This perspective – this way of representing the physics – gives windspeed and turbulence profiles which capture some of the important trends seen in experiments and high-fidelity CFD analyses. The resolution of the simplified boundary-layer method

Table II: A comparison of default (at left) and optimal (at right, to the nearest 0.2 deg) pitch settings in a large turbine array, with the objective of maximizing production. The array is 11 turbines deep, and infinitely wide. The terrain is flat, the ambient hub-height windspeed is 10 m/s, and turbine spacing is a uniform 8*D*. Pitch angles are given in degrees, hub-height windspeed in m/s, and power in MW per column of turbines.

Turbine	β	V_h	I	P	β	V_h	I	P
1	0.0	10.00	0.086	7.106	1.0	10.00	0.086	7.033
2	0.0	9.60	0.101	6.371	1.0	9.62	0.101	6.344
3	0.0	9.36	0.113	5.902	1.0	9.39	0.111	5.900
4	0.0	9.17	0.121	5.563	1.0	9.21	0.119	5.576
5	0.0	9.03	0.127	5.301	1.0	9.07	0.125	5.326
6	0.0	8.91	0.131	5.094	1.0	8.96	0.129	5.126
7	0.0	8.81	0.134	4.926	0.6	8.86	0.132	4.992
8	0.0	8.72	0.137	4.787	0.6	8.77	0.134	4.845
9	0.0	8.65	0.138	4.670	0.4	8.70	0.136	4.734
10	0.0	8.59	0.140	4.571	0.0	8.63	0.138	4.639
11	0.0	8.54	0.141	4.485	0.0	8.57	0.140	4.538
Total				58.775				59.052

is coarse, not accounting for the precise placement of turbines relative to the wind; rather, it gives results which are valid for winds averaged over a sector of some degrees. This is not as severe assumption as it may seem, since the wind direction in a large wind power plant is, in reality, not a perfectly consistent and definable quantity.

Approximating the influence from one turbine to the next by constant coefficients, whose values are a function of the particular turbine operation, spacing, and mean flow conditions, a linear approximation to the boundary-layer analysis is obtained. Dynamic flow is added to the linear steady-state analysis by, first, using an effective value of thrust, based on dynamic induced velocity in the rotor wake; and second, considering the convection delay from one turbine to the next.

The present engineering method is intended for preliminary design and tuning of wind power plant controllers, as well as for generating hypotheses which may be tested by experiments and more refined analyses.

References

[1] Frandsen ST, *et al*. (2009). The making of a second-generation wind farm efficiency model complex. Wind Energy 12:445-458.

[2] Ainslie JF (1988). Calculating the flowfield in the wake of turbines. Journal of Wind Engineering and Industrial Aerodynamics 27:213-224.

[3] Merz KO (2014). VIPER: A tool for computing energy production from large offshore wind farms. Report TR A7382, SINTEF Energy Research, Norway.

[4] Larsen GC, *et al*. (2007). Dynamic wake meandering modeling. Report Risø-R-1607(EN), Risø National Laboratory, Denmark.

[5] Belcher SE, *et al*. (2003). Adjustment of turbulent boundary layer to a canopy of roughness elements. Journal of Fluid Mechanics 488:369-398.

[6] Frandsen ST (2007). Turbulence and turbulence-generated structural loading in wind turbine clusters. Report Risø-R-1188(EN), Risø National Laboratory, Denmark.

[7] Merz KO (2015). A linear state-space model of an offshore wind turbine, implemented in the STAS wind power plant analysis program. Report TR A7474, SINTEF Energy Research, Norway.

[8] Pedersen M (2016). Steady and transient inflow dynamics with actuator disk vortex theory. Manuscript submitted to Wind Energy.

[9] Annoni J, *et al*. (2016b). An experimental investigation on the effect of individual turbine control on wind farm dynamics. Wind Energy 19:1453-1467.

[10] Burton T, *et al*. (2001). *Wind Energy Handbook*. Chichester: Wiley.

[11] Snel H, Schepers JG (1995). Joint investigation of dynamic inflow effects and implementation of an engineering method. Report ECN-C--94-107, Energy Research Centre of the Netherlands.

[12] Bak C, *et al*. (2013). Description of the DTU 10 MW Reference Wind Turbine. DTU Wind Energy Report-I-0092, Technical University of Denmark.

[13] Hansen KS (2013). Presentation of Nørrekær Enge wind farm and Nordtank 300kW wind turbine. Report by the Technical University of Denmark for IEA Wind Task 31: Wakebench.

[14] Chamorro LP, Porté-Agel F (2009). A wind-tunnel investigation of wind-turbine wakes: boundary-layer turbulence effects. Boundary-Layer Meteorology 132:129-149.

[15] Jensen NO (1983). A Note on Wind Generator Interaction. Report Risø-M-2411, Risø National Laboratory, Denmark.

[16] Machielse LAH, *et al*. (2007). Evaluation of "Heat and Flux" Farm Control – Final Report. Report ECN-E--07-105, Energy Research Centre of the Netherlands.

[17] Annoni J, *et al*. (2016a). Analysis of axial-induction-based wind plant control using an engineering and a high-order wind plant model. Wind Energy 19:1135-1150.